	Form Approved OMB NO. 0704-0188

1. AGENCY USE ONLY (Leave Blank)	2. REPORT DATE	3. REPORT TYPE AND DATES COVERED
	17-May-2007	Final 15-May-2006 to 14-Feb-2007

4. TITLE AND SUBTITLE	5. FUNDING NUMBERS
Development of Targeting UAVs Using Electric Helicopters and Yamaha RMAX	W911NF-06-1-0152
6. AUTHOR(S) S. Sastry, D. Shim, H. Chung	
7. PERFORMING ORGANIZATION NAME(S) AND ADDRESS(ES) University of California - Berkeley Sponsored Projects Office\	8. PERFORMING ORGANIZATION REPORT NUMBER
9. SPONSORING / MONITORING AGENCY NAME(S) AND ADDRESS(ES) U. S. Army Research Office P.O. Box 12211 Research Triangle Park, NC 27709-2211	10. SPONSORING / MONITORING AGENCY REPORT NUMBER 50581.1-CI-II

11. SUPPLEMENTARY NOTES

The views, opinions and/or findings contained in this report are those of the author(s) and should not be construed as an official Department of the Army position, policy or decision, unless so designated by other documentation.

12 a. DISTRIBUTION / AVAILABILITY STATEMENT	12 b. DISTRIBUTION CODE
Approved for public release; distribution unlimited.	

13. ABSTRACT (Maximum 200 words)

Unmanned aerial vehicles (UAVs) are ideal for such scenarios with high risk and heavy workload requiring a great accuracy beyond human capability. Target designation is a good example of such tasks. The task without a secondary actuator is not equal to typical hovering that pilots are trained for and the required accuracy is too high for human pilots. Further, large manned rotorcraft have high inertia and sluggish control response, and therefore the hovering accuracy is no match to that of smaller UAVs. In this project, we developed high-precision targeting system without a secondary actuation system through the precision control of the vehicle itself. For error analysis and control law design, we first derive the equation to find the end-point coordinates on the target and then extract the control objective to keep the laser sight with minimal jitter. The control metric for targeting is shown to differ from typical hover due to the dynamics of helicopters. A new lightweight and agile helicopter platform is developed with compact yet potent avionics, which can be easily transferred to other rotorcraft systems like Yamaha RMAX. A sample test mission is defined and the flight data is used for quantitative analysis.

14. SUBJECT TERMS	15. NUMBER OF PAGES
laser target designation, helicopter uav, precision hovering	15
	16. PRICE CODE

17. SECURITY CLASSIFICATION OR REPORT	18. SECURITY CLASSIFICATION ON THIS PAGE	19. SECURITY CLASSIFICATION OF ABSTRACT	20. LIMITATION OF ABSTRACT
UNCLASSIFIED	**UNCLASSIFIED**	**UNCLASSIFIED**	**UL**

NSN 7540-01-280-5500

Standard Form 298 (Rev.2-89)
Prescribed by ANSI Std. 239-18
298-102

Development of Targeting UAVs Using Electric Helicopters and Yamaha RMAX

Final Report

May 2007

David Hyunchul Shim, Hoam Chung, and Shankar Sastry

University of California, Berkeley

Table of Contents

Table of Figures

I. Introduction

There are many situations that airborne platforms need to point a camera or a laser source to a ground target, either stationary or moving. For aerial still-imaging or live-video relaying, the camera should be held consistently pointing to the target regardless of the host vehicle's motion. For target designation, the rolling of the beam is less critical, but the laser beam should be on the target without much deviation over time. Typically, high-precision targeting or image stabilization is achieved by an add-on gimbal system. Secondary actuators cancel out the vehicle's translation and rotation sensed by accelerometers and gyros in the gimbal system. For fixed-wings, due to the nonzero speed of the host vehicle during the flight, maintaining a good lock is usually very difficult or impossible without a help of such devices. For rotary-wing aircraft, however, the pointing task is somewhat achievable if the vehicle is allowed to hover. However, it requires the vehicle to remain stationary with great accuracy, which is not always possible especially when the vehicle is exposed to a significant threat. Even if the vehicle is allowed to do so, it poses a heavy burden on the pilot.

Unmanned aerial vehicles (UAVs) are ideal for such scenarios with high risk and heavy workload requiring a great accuracy beyond human capability. Agile UAVs with accurate sensors are capable of precision flight control that can be very difficult to human pilots. Target designation is a good example of such tasks. The "lasing" task without a secondary actuator is not equal to typical hovering that pilots are trained for and the required accuracy is too high for human pilots. Further, large manned rotorcraft have high inertia and sluggish control response, and therefore the hovering accuracy is no match to that of smaller UAVs. In this project, we developed high-precision targeting system without a secondary actuation system through the precision control of the vehicle itself.

For error analysis and control law design, we first derive the equation to find the end-point coordinates on the target and then extract the control objective to keep the laser sight with minimal jitter in Section II. In this process, the control metric for targeting is shown to differ from typical hover due to the dynamics of helicopters. A regulating control problem is formulated in Section II. A new lightweight and agile helicopter platform is developed with compact yet potent avionics, which can be easily transferred to other rotorcraft systems like Yamaha RMAX. A sample test mission is defined and the flight data is used for quantitative analysis in Section IV. The conclusion and future works are given in Section V.

II. Formulation

In this section, we first derive a geometric relationship of the projected point of a straight beam projected on a target from a source mounted on a vehicle. From this relationship, the control objective is formulated. Then we find a control law to achieve the objective.

A. End-point coordinates of projected beam

In this research, we consider a targeting problem where a light source rigidly attached to the vehicle's frame projects a beam spot on a target. The end-point is defined as the intersecting point of the straight line representing the path of the laser beam and the surface of the target. Although a target would have an arbitrary complex shape, however, without loss of generality, we first consider a wall perpendicular to the level ground. It is also assume that the vertical wall is initially perpendicular to the heading direction of the vehicle. The light source emits a beam that travels along a line, which we assume to lie on the X^B-Y^B plane (therefore X^L-Y^L plane as well) and intersect X^B with angle α as depicted in Figure 1.

The body coordinates can be converted to the local Cartesian (or spatial) coordinates (in north-east-down direction), indicated by superscript *B* and *S* respectively, using the following unitary transformation

$$\mathbf{R}^{B/S} = \begin{bmatrix} \cos\Psi\cos\Theta & \sin\Psi\cos\Theta & -\sin\Theta \\ -\sin\Psi\cos\Phi + \cos\Psi\sin\Theta\sin\Phi & \cos\Psi\cos\Phi + \sin\Psi\sin\Theta\sin\Phi & \cos\Theta\sin\Phi \\ \sin\Psi\sin\Phi + \cos\Psi\sin\Theta\cos\Phi & -\cos\Psi\sin\Phi + \sin\Psi\sin\Theta\cos\Phi & \cos\Theta\cos\Phi \end{bmatrix} \quad (1)$$

where the superscript *B/S* indicates the transformation from spatial to body coordinate systems. (Φ, Θ, Ψ) are roll, pitch, yaw angles of *ZYX* Euler angle representation, respectively. Similarly, the transformation from the laser source to the body coordinate system can be computed by the following transformation,

$$\mathbf{R}^{B/L}(\alpha) = \begin{bmatrix} \cos\alpha & 0 & -\sin\alpha \\ 0 & 1 & 0 \\ \sin\alpha & 0 & \cos\alpha \end{bmatrix}. \quad (2)$$

The straight line of the laser beam in the three-dimensional space can be described as

$$\begin{aligned} \mathbf{X}_P^S &= \mathbf{X}_{D/L}^S + \mathbf{X}_{L/B}^S + \mathbf{X}_H^S \\ &= \mathbf{R}^{S/B}\mathbf{R}^{B/L}(\alpha)\mathbf{X}_{D/L}^L + \mathbf{R}^{S/B}\mathbf{X}_{L/B}^B + \mathbf{X}_H^S \,, \\ &= q\mathbf{R}^{S/B}\mathbf{R}^{B/L}(\alpha)\mathbf{u}_X^L + \mathbf{R}^{S/B}\mathbf{X}_{L/B}^B + \mathbf{X}_H^S \end{aligned} \quad (3)$$

where $q \in \mathbf{R}^+$ and $\mathbf{u}_X^L$ is the unit vector in the direction of laser beam in the laser source coordinate system denoted as *L*.

The end-point on the target surface is defined as the intersection of the straight line (Eq. (3)) and the target surface in Figure 1. Once the platform-specific parameters such as α and $\mathbf{X}_{L/B}^B = (x_l, 0, z_l)$ are given, we can solve for the intersection point on the target plane. For the sake of simple but insightful analysis, we assume the target plane lies in Y^S-Z^S plane and passes $(L, 0, 0)$ in the spatial coordinates and the helicopter has nominally zero heading angle[1] as given in Figure 1. Then one can find the unknown parameter q[2], along with the coordinates of the end-point on the target plane, with given helicopter position $\mathbf{X}_H^S = (x_H, y_H, z_H)$ and rotation vector (Φ, Θ, Ψ).

By letting $X_P^S = X_D^S = (L, y_P, z_P)$, we can solve for an exact solution, which is unique and straightforward from the following:

$$\begin{bmatrix} L \\ y_P \\ z_P \end{bmatrix} = q\mathbf{R}^{S/B}\begin{bmatrix} \cos\alpha \\ 0 \\ \sin\alpha \end{bmatrix} + \mathbf{R}^{S/B}\begin{bmatrix} x_L \\ 0 \\ z_L \end{bmatrix} + \begin{bmatrix} x_H \\ y_H \\ z_H \end{bmatrix} \quad (4)$$

The solution can be obtained after a lengthy manipulation. For analysis, we wish to obtain simpler yet insightful approximation by introducing small-angle assumptions into Eq. (1) such that

[1] For a more general case of having arbitrary heading, one can easily introduce a rotation matrix that accounts for the nonzero heading.

[2] q is the distance that the beam travels before hitting the wall.

$$\mathbf{R}^{S/B} \approx \begin{bmatrix} 1 & -\Psi & \Theta \\ \Psi & 1 & -\Phi \\ -\Theta & \Phi & 1 \end{bmatrix} \tag{5}$$

Also, $\mathbf{X}_{L/B}^{B} = (x_L, 0, z_L)$ is very small comparing with the distance from the target so it is also ignored. Then we have

$$\begin{bmatrix} L - x_H \\ y_P - y_H \\ z_P - z_H \end{bmatrix} \approx q \begin{bmatrix} \cos\alpha + \Theta\sin\alpha \\ \Psi\cos\alpha - \Phi\sin\alpha \\ -\Theta\cos\alpha + \sin\alpha \end{bmatrix} \tag{6}$$

By arranging Eq. (6), we have

$$\begin{bmatrix} y_P \\ z_P \end{bmatrix} \approx \begin{bmatrix} y_H + q(\Psi\cos\alpha - \Phi\sin\alpha) \\ z_H + q(-\Theta\cos\alpha + \sin\alpha) \end{bmatrix} \tag{7}$$

where

$$q \approx \frac{L - x_H}{\cos\alpha + \Theta\sin\alpha} \approx \frac{L - x_H}{\cos(\alpha - \Theta)} \tag{8}$$

The result of Eq. (8) is intuitive from Figure 1. During the target designation, the overspill angle is substantially larger than the pitch angle near zero, $\alpha \gg \Theta$ and Eq. (7) reduces further to

$$\begin{bmatrix} y_P \\ z_P \end{bmatrix} \approx \begin{bmatrix} y_H + (L - x_H)(\Psi - \Phi\tan\alpha) \\ z_H + (L - x_H)(-\Theta + \tan\alpha) \end{bmatrix} \tag{9}$$

The simplified result in Eq. (9) shows an approximated relationship of the end-point coordinate in terms of the helicopter's position attitude deviation. By applying the differential operator δ to Eq. (9) and ignoring second order terms, we have

$$\delta y_P = \delta y_H + L\delta\Psi - L\tan\alpha\delta\Phi \tag{10}$$

$$\delta z_P = \delta z_H - L\delta\Theta - \delta x_H \tan\alpha \tag{11}$$

From Eq. (10) and (11), we discover the followings:

- As expected, the end-point deviation is coupled with the helicopter's position and attitude change.
- The horizontal deviation is mainly affected by the vehicle's deviation in lateral direction, heading, and roll angle.
- The vertical deviation is mainly affected by the vehicle's deviation in longitudinal and vertical directions and pitch angle.
- Since the distance from the target is much greater than the perturbation of the helicopter's position, the end-point deviation is more heavily affected by the angular perturbation than the linear counterpart. For example, one meter of horizontal or vertical deviation is equivalent with only 0.57°of heading or pitch angle change, respectively, if L=100 meters.
- The impact of attitude variation becomes stronger with larger distance L.

Similarly, if the target is assumed to be a flat region on the ground (area target), the end-point is projected on the ground. One can find the relationship of the perturbed end point by letting $X_P^S = X_D^S = (x_p, y_p, 0)$ such that

$$\delta x_P = \delta x_H - \delta z_H \sec\alpha - z_H \delta\Theta \tag{12}$$

$$\delta y_P = \delta y_H - z_H \sec\alpha \delta\Psi + z_H \delta\Phi \tag{13}$$

From Eq. (12) and (13), similar observations can be drawn. For ground target, as α becomes smaller, the targeting becomes a shallower overspill and therefore the accuracy is degraded further by (sec α) term. The error is also dependent on the altitude of the helicopter, not just its change.

B. Control Strategy

Helicopters are well known to be an underactuated system, which means there are fewer actuation inputs than the number of degree of freedom. Therefore, the resulted motion is constrained in $\mathbf{R}^3 \times SO(3)$ manifold. With the standard configuration of main-tail rotors, the helicopter can roll, pitch, yaw, and heave as the direct outcome of manipulating the control surfaces. The horizontal motion in longitudinal and lateral direction is achieved by first pitching and rolling of the vehicle, respectively.

Typically, a precision hover is defined as minimal deviation in the position and the heading:

$$\min \left\|\delta x_H\right\|_2^2 + \left\|\delta y_H\right\|_2^2 + \left\|\delta z_H\right\|_2^2 + \left\|\delta\Psi\right\|_2^2, \tag{14}$$

where $\left\|\square\right\|_2$ indicates the Euclidian norm. In Eq. (14), the vertical position and heading can be directly controlled by the main and tail rotors' collective pitch inputs, respectively, the horizontal motion is achieved by first giving rolling or pitching commands. In this process, the rolling and pitching angles are bound to be perturbed and therefore the targeting accuracy is affected as shown in the previous subsection. When a secondary stabilization platform is employed, the control problem becomes decoupled and almost trivial, since the angular perturbation can be actively compensated for by the gimbal, which typically has much faster response time and accuracy than the vehicle's motion itself. To repeat, however, such devices are expensive and our goal is to find a lower-cost alternative to achieve acceptable targeting accuracy without such platforms.

Therefore, in order for a high quality target designation, the control objective is given as (vertical wall case)

$$\begin{aligned} &\min \left\|\delta y_P\right\|_2^2 + \left\|\delta z_P\right\|_2^2 \\ &= \min \left\|\delta y_H + L\delta\Psi - L\tan\alpha\delta\Phi\right\|_2^2 + \left\|\delta z_H - L\delta\Theta - \delta x_H \tan\alpha\right\|_2^2 \end{aligned} \tag{15}$$

Examining Eq. (10) and (11), we find that δy_P and δz_P are not coupled in terms of the control input as explained later. Therefore, the minimization can be performed on each axis in a decoupled manner. Eq. (15) is a regulation problem and it can be written in linear quadratic regulation (LQR) form, or, can be dynamically solved over a finite horizon using the framework of model predictive control[4].

Suppose a dynamic system model of a helicopter in hover can be approximated by a linear difference equation such that

$$
\begin{aligned}
x(k+1) &= Ax(k) + Bu(k) \\
y(k) &= Cx(k) \\
&= \begin{bmatrix} \delta x_H & \delta y_H & \delta z_H & \delta\Phi & \delta\Theta & \delta\Psi \end{bmatrix}^T
\end{aligned}
\quad ., \tag{16}
$$

where x is the system variable and u is the input to the system. A system model example can be found by a system identification process in a similar way presented in Ref. 2.

When we consider a LQR or MPC, the cost function $L(x,u)$ can be expressed as

$$
L(x,u) = x^T Q x + u^T R u \,, \tag{17}
$$

where

$$
\begin{aligned}
Q &= C^T \begin{bmatrix} M^T M & 0 \\ 0 & N^T N \end{bmatrix} C \\
M &= diag\{0,1,0,-L\tan\alpha,0,L\} \\
N &= diag\{-\tan\alpha,0,1,0,-L,0\}
\end{aligned}
\tag{18}
$$

As well known from the LQ control theory, with given system equation, one can find a stabilizing controller with the given Q and a positive definite R.

III. Testbed Development

In this section, we introduce the vehicle platform, hardware, and software architecture developed for the target designation task. It is developed as a multi-purpose proof-of-concept testbed for various algorithms in classical GN&C as well as advanced multi-agent coordination.

A. Vehicle Platform

The testbed used in this research is based on an electrically powered radio control helicopter, whose detailed specification is given in Table 1. The onboard components are designed and integrated with emphasis on the volume and weight reduction for longer flight time, maneuverability and reliability. An extra effort is made to keep the onboard system compact so that the original canopy can be retained in order to enhance the visibility of and the aerodynamic characteristics of the vehicle. We also avoided using an oversized landing gear that are commonly used elsewhere to mount the avionics because it

Figure 1. A snapshot of the targeting testbed during autonomous flight

significantly increases the overall vehicle inertia and weight, not to mention it is less aesthetically favorable. Instead, we use a heavy-duty, regular size landing gear and mounted the avionics at the end of the main fuselage as shown in Figure 1. The center of mass shift due to the introduction of the avionics is countered by adding more batteries at the nose of the helicopter, thus significantly increasing the flight time. The DC brushless motor with high-capacity Lithium-ion-polymer batteries allows for more than 20 minutes of continuous flight. The electric power plant can easily start and stop by fully remote operation. As well known, the Lithium-polymer batteries can be easily damaged or even explode if overly discharged below its minimum voltage of 3.3V per cell. Therefore an onboard battery monitor circuit is added to monitor the voltage, current, watt, and the consumed energy so that the mission is aborted before the battery is drained beyond the allowable limit.

The electronic motor and the onboard electronics are powered by the same Lithium polymer battery pack, therefore eliminating the need to carry a separate battery pack to power the electronics. The onboard electronics consumes only a very small fraction(<5%) of the charge comparing with the power-hungry electronic motor. However, we kept a separate battery to power the radio receiver and the servomotors to allow safe take-over of the vehicle even when the main battery ceases to supply power.

The avionics enclosure contains PC104-based computer stack (2 layers), NovAtel GPS OEM V-2, 900MHz Ethernet Bridge, a wireless modem, an isolated DC/DC converter, a video overlay board, and a multi-function interface board (MFIB). Although there are many smaller embedded processors available, we prefer a Pentium-based CPU for its sheer processing power, compatibility, and the availability of many operating systems including the QNX real-time operating system. The video overlay board is useful to display the onboard camera's image with important information such as the vehicle's coordinates, attitude, heading, system status and so on. The MFIB, measuring 8cm×4.5 cm, is a highly integrated custom-design interface board based on two 16F873A PIC microprocessors, which communicate with the CPU board through a bi-directional serial port. They are responsible for reading and generating multiple PWM signal channels and also reading absolute/differential pressure sensors and a temperature sensor. It also provides a serial interface to communicate with the battery monitoring system mentioned above.

The avionics is tightly integrated in a small enclosure of 5"×5"×3" made of aluminum to reduce EMI radiation, which may cause the jamming of the radio signal from the radio control transmitter. During the fully autonomous operation, the manual control signal is not critical, but we opt to keep the channel fully operational to use it as the last resort to recover the vehicle if the avionics fails beyond its capability of self-recovery. We prefer using mechanical relays to physically switch the servo signal between the radio control receiver and the flight computer because, if all system fails and the power is lost, the mechanical relay will be de-energized and the manual control loop will be immediately recovered.

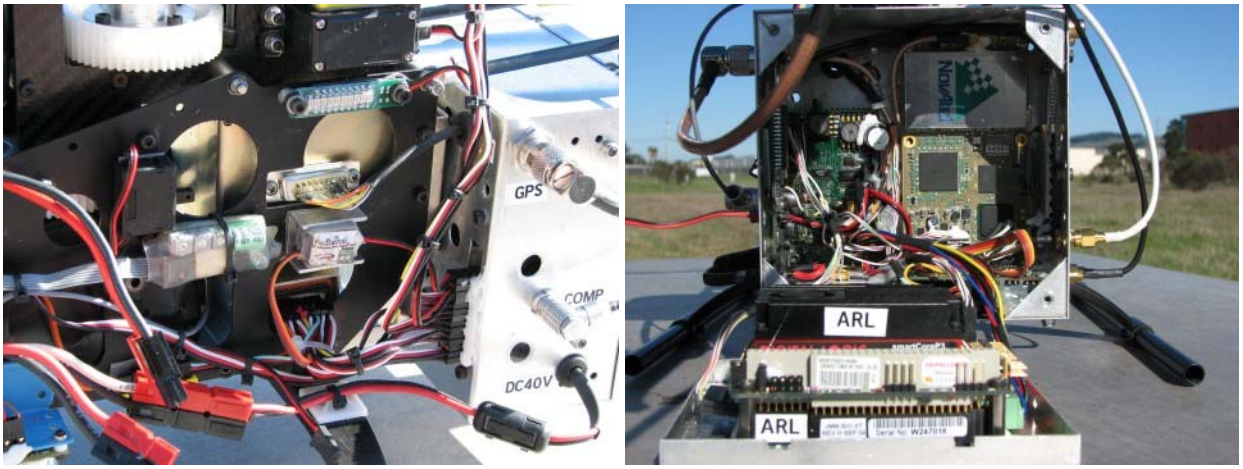

Figure 2. Detailed views of Maxi-Joker based laser targeting UAV

Table 1. Specification of a Berkeley UAV testbed

Base platform	Electric Helicopter (Maxi-Joker)
Dimensions	0.26 m(W) × 2.2 (L) × 0.41 (H)
Rotor Diameter	1.8 m
Weight	7.5 kg (fully instrumented)
Powerplant	Actro 32-4 motor (1740W max at 75A) Lithium-Ion-Polymer (10S6P; 40V 12Ah)
Operation Time	20 minutes
Avionics	Navigation: DGPS-aided INS GPS:NovAtel OEM V-2 IMU: Inertial Science ISIS IMU Flight Computer: PC104 Pentium III 700MHz Communication: - 900MHz Ethernet Bridge (Telemetry,1Mbps) - Radio Modem (DGPS broadcast, <115Kbps)
Autonomy	Waypoint navigation with automatic VTOL Position-tracking servo mode MPC-enabled dynamic path planning with collision avoidance Stability-augmentation system

The inertial measurement unit (IMU) is hard mounted between the aluminum walls of the fuselage outside of the avionics enclosure. Owing to the smaller level of vibration from the electric motor, the IMU does not need special shock damping. Additional benefit is the improved cooling, which is nice to keep the thermal drift of the inertial sensors smaller. The navigation solution is obtained by running our custom inertial navigation algorithm running at 100Hz, combined with the high-precision DGPS correction at 5Hz. The primary communication between the ground computer and the onboard computer is enabled by a 900MHz Ethernet bridge at 1Mbps. The DGPS correction data is relayed by additional wireless modem. The flight data is transmitted to the ground station, and optionally stored on the ground computer for future retrieval. The vehicle is also equipped with a digital compass for initial heading alignment and a set of ultrasound sensors to measure the relative distance to the ground for autonomous landing. Detailed pictures of the final assembly of the Maxi-Joker-based UAV are shown in Figure 2.

B. Software

The flight control software is implemented on QNX, a commercial real-time operating system. Fully utilizing the built-in multi-processing architecture with inter-process synchronization and communication mechanisms, the software consists of a number of modules with dedicated periodic tasks at diverse rates. The processes are synchronized using a QNX-proprietary inter-process communication (IPC) mechanism called *proxy.* The data communication between processes is facilitated with s*hared memory*, protected by associated mutual exclusion flags.

The flight control software shown in Figure 3 functions through the collaboration of concurrently running processes, BEARNAV, GPS, COMM, and SERVOREAD*,* which are named after their own responsible tasks. The flight software is architected to be faithful to every pilot's mantra, "*aviate, navigate, and communicate".* A pilot's foremost goal is to keep the aircraft stably in the air, and then perform the mission, and then report the current status and listen to the command. Therefore the BEARNAV, the most important process in charge of computing the navigation solution and the stabilizing control input to the vehicle, is written to be free from any potentially blocking calls. The blocking-prone communication task is delegated by a process COMM, which receives the communication

request from other processes and sends them when the CPU is freed from the flight-critical processes. The GPS process is in charge of reading the serial input from the GPS and reporting the decoded information to BEARNAV. SERVOREAD is responsible for reading the pilot's manual radio control signal, which is used for system identification or the feedforward command when the helicopter is operated in stability-augmented mode. At every 10ms, BEARNAV computes the navigation solution using the IMU data received and continues to run the feedback control routine.

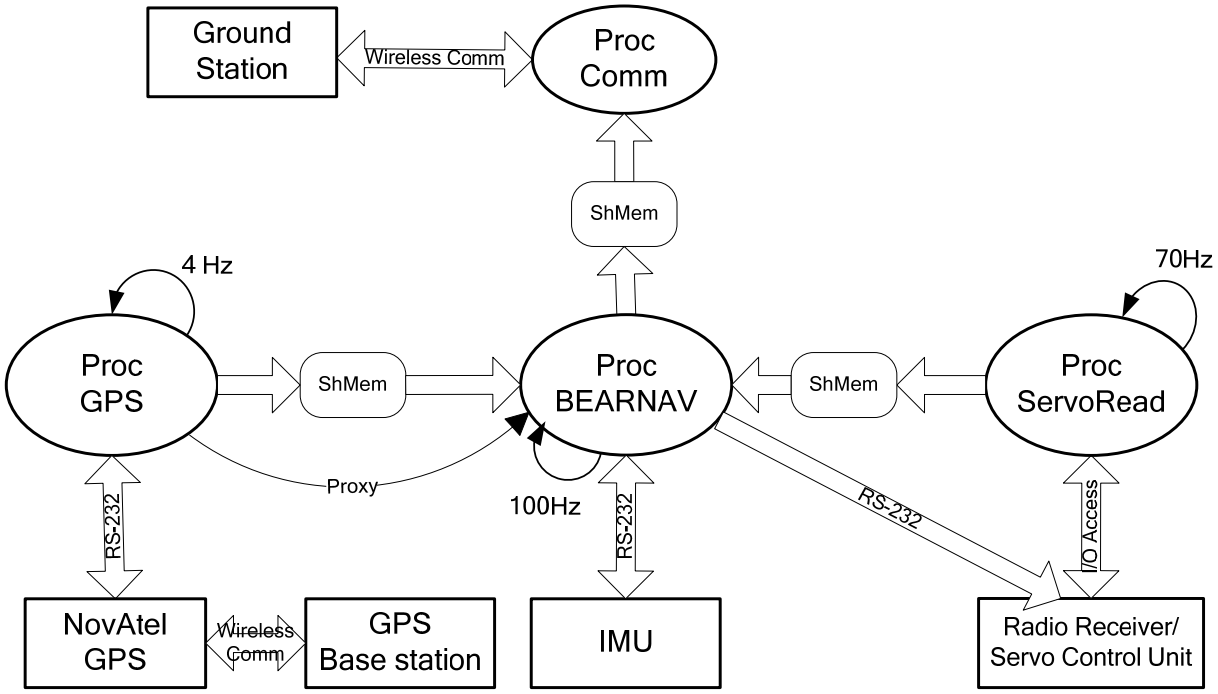

Figure 3. Flight control software architecture

The Berkeley UAV fleet consists of a number of experimental testbed UAVs based on different vehicle platforms, configured for research and development of vehicle control[2], multi-agent coordination[5] and advanced sensor systems[6] and more. Although we intend to maintain common set of components as much as possible, each vehicle has a different combination of hardware and platform. In order to maintain a common flight control software structure that can be easily recompiled without losing the core capability, our onboard software utilizes a header file that specifies a specific combination of onboard components and also the vehicle's control settings. For each component, a class library is written with a standard interface defined. The resulted software is therefore guaranteed to be fully customized with the target vehicle's configuration while preserving the common functionalities such as control strategies and communication protocols.

IV. Experiment Results

In this section, we present the experiment results of the proposed UAV system. We first introduce a targeting scenario and present experiment results, which is discussed in detail in light of the results in Section II. We begin with a scenario where a helicopter UAV takes off, flies to an altitude to assess the situation, flies towards the target, *lases* the target, and returns to the base. Figure 4 illustrates this scenario. During the target designation, the vehicle is 100 meters away in horizontal direction, and 30 meters high

above from the target, which is assumed as a vertical wall as discussed in Section II. In this configuration, the laser source needs to be inclined by 16.7°, which is rather a shallow spill.

We begin by collecting a flight data set to validate the ideas proposed in Section II. To guide the vehicle to realize the given scenario, the flight sequence is programmed by VCL[2], which allows describing a waypoint-based mission in a readable script language form. The waypoint is specified with corresponding flight mode command such as take-off, hover, or cruise with optional parameters such as speed or heading. A VCL script for the scenario given in Figure 4 is list below. As can be inferred from the script, it commands in the following sequence that contains the sample scenario.

- Take-off
- Initial horizontal flight to take the vehicle away from the launching point at 3m/s
- Ascent to 60 m AGL at 4m/s vertical
- Hover at the target detection point for 15 sec.
- Forward flight to the target designation point at 4m/s
- Hover at target designation point for 10 seconds
- Fly back to the target detection point at 4m/s
- Hover for 11 seconds
- Descent by 54 meters at 3m/s
- Fly back to the launching point at 3m/s
- Hover for 5seconds
- Land

```
TakeoffTo (0,0,-3)rel vel=1m/s autoheading;
Hover duration=5sec;
FlyTo (50,30,-3)rel vel=3m/s autoheading;
FlyTo (0,0,-54)rel vel=4m/s heading=180deg;
Hover (0,0,0)rel heading=180deg duration=15sec;
FlyTo (-100,0,30)rel vel=4m/s heading=180deg;
Hover (0,0,0)rel heading=180deg duration=11sec;
FlyTo (100,0,-30)rel vel=4m/s autoheading;
Hover duration=10sec;
FlyTo (0,0,54)rel vel=3m/s;
FlyTo (-50,-30,3)rel vel=3m/s autoheading;
Hover duration=5sec;
Land (0,0,*)rel;
```

<< Corresponding VCL Script>>

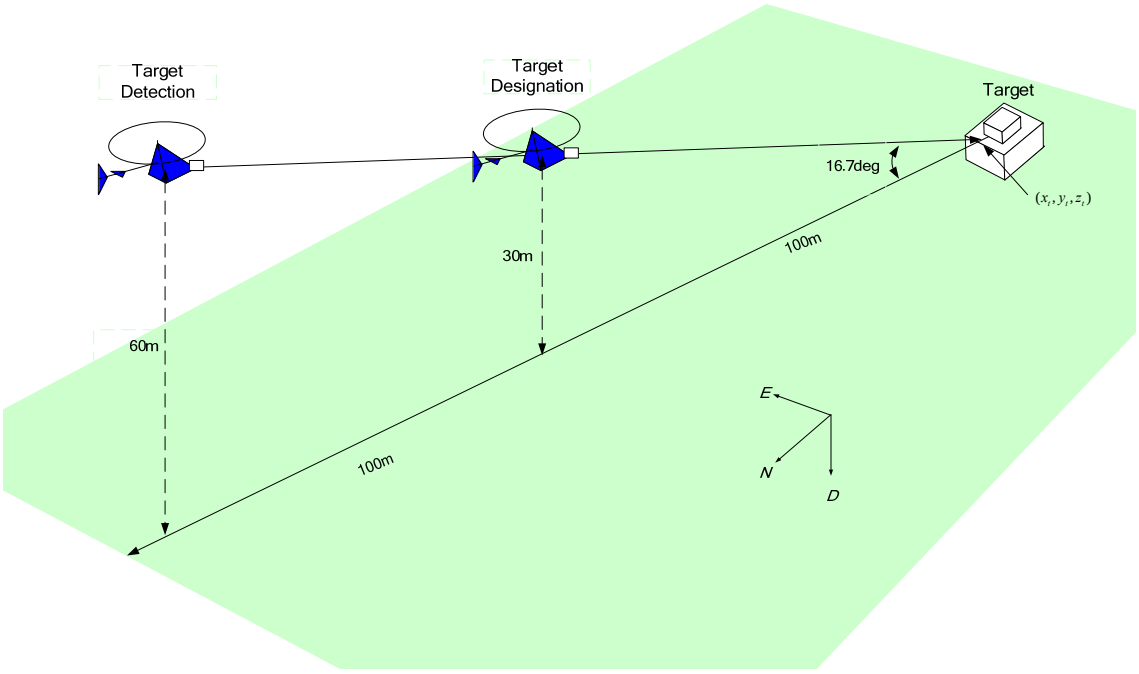

Figure 4. An illustration of a sample target designation

The experiment was performed using the small helicopter UAV introduced in Section III. The experiment was performed on a calm cloudy day. The air temperature was about 14°C. The experiment data over the entire flight path is also given in Figure 4. The flight data when the helicopter is at the target

designation point is put under a close examination. In Figure 5, a detailed flight data during the designation is given. During the hover for a little more than 10 seconds, the helicopter deviated 0.269 m, 0.344 m, and 0.049 m in *X*, *Y*, and *Z*-direction, respectively. In angular motion, the helicopter showed 3.63°, 3.23°, and 2.11° in roll, pitch, and yaw direction, respectively. This is in general regarded as a very good hovering flight.

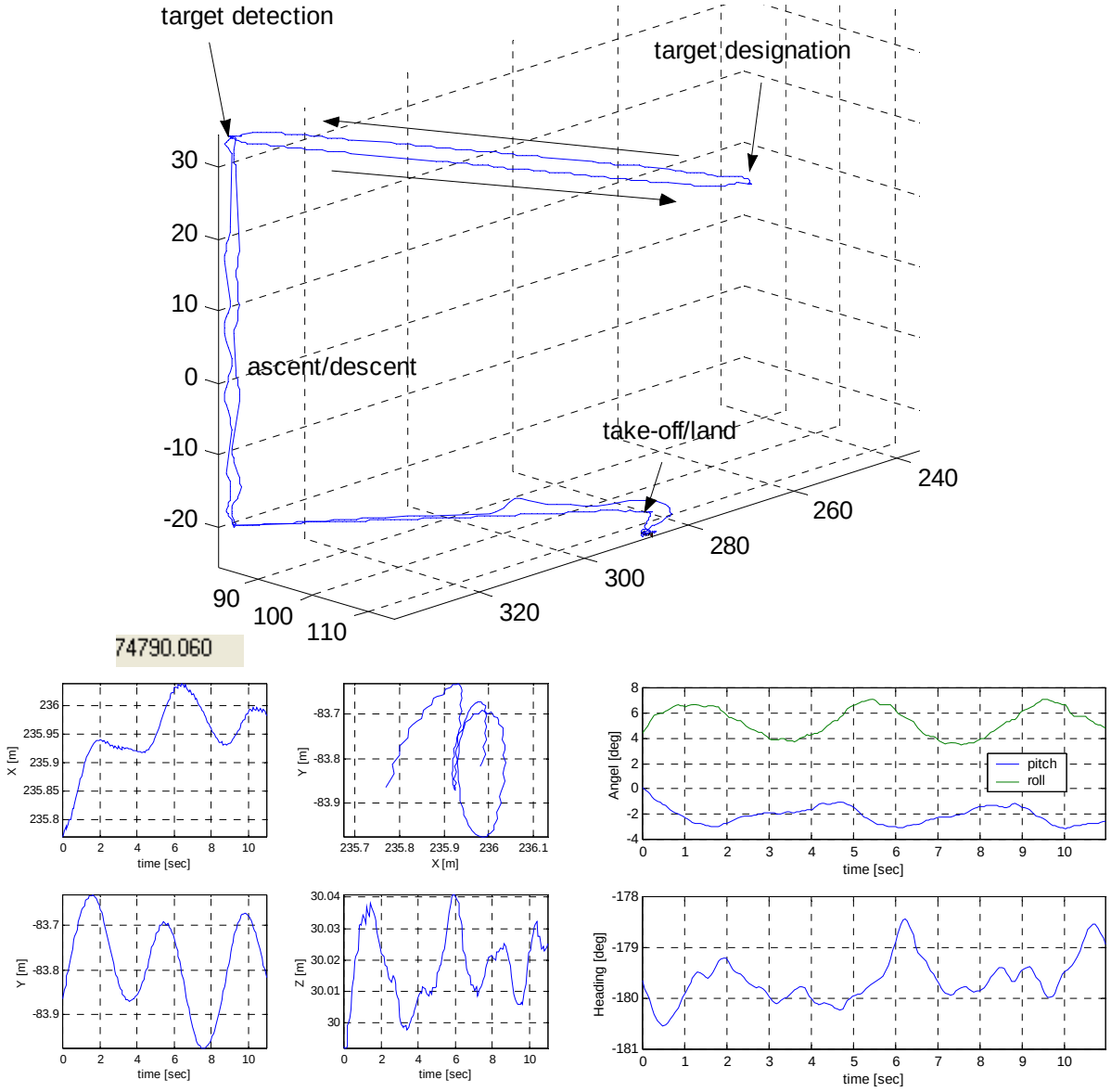

Figure 5. An experiment result of the proposed scenario

Eq. (4) can be used to compute the coordinates of the end-points. In Figure 6, the exact solution of end-points are plotted together with those computed by with approximated solutions Eq. (7), (10) and (11). It is also observed that the approximate solutions give fairly accurate estimates in *Y* direction, but Z-direction component is somewhat smaller than the exact solution. It is attributed to the neglected pitch angle to compute *q*. During the hover, the end-point is contained in a box of 5 meters in horizontal direction and 6 meters in vertical direction. For further analysis, we examine the contributing portion of

each term as shown in Figure 7. Using Eq. (10) and (11), estimate the contributions of each term to the end-point deviation are computed and plotted as shown in Figure 6. For horizontal error, the perturbation in yaw direction has the large contribution while the roll angle also contributes somewhat less but substantially as well. The yaw deviation can be improved by bypassing the hobby-grade rate gyro and use the high-quality IMU data instead for more reliable and accurate heading control. For vertical error, the perturbation of pitch angle is the most dominant contributor. From Figure 7, the pitch angle deviates no more than 4 degrees yet it causes a large deviation as shown in Figure 7. Therefore, we propose, in our following work in near future, to use the regulating controller using Eq. (17) and (18). Simulation and flight tests will be performed very soon.

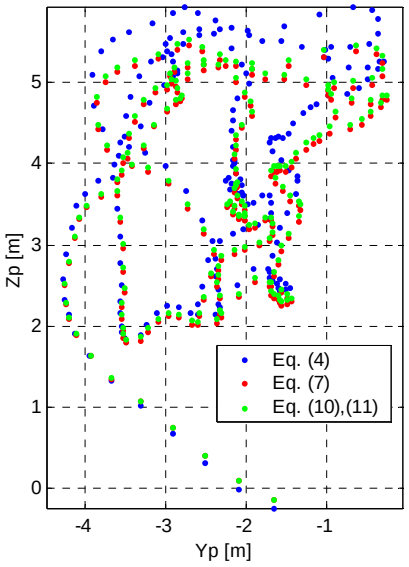

Figure 6. End-point plots using exact and approximate solutions

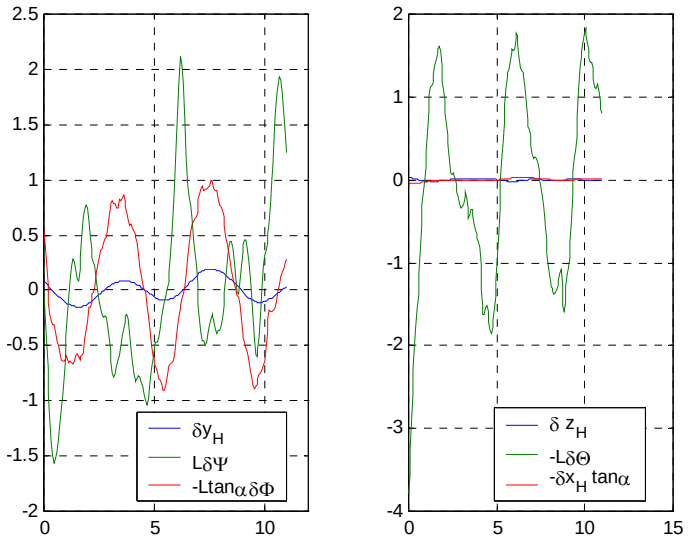

Figure 7. Contribution of error terms (left: horizontal error, right: vertical error)

V. Extension to Yamaha RMAX

The work presented here so far was conducted on an electrically powered radio controlled helicopter, Maxi Joker 1. The full-scale laser targeting experiment at Yuma proving ground (YPG) will be performed using Yamaha RMAX, which will provide sufficient payload to carry the laser target designator (~5kg) and other associated components. Our Berkeley UAV testbeds have been designed to provide maximal compatibility of the flight software when the target configuration changes from vehicle to vehicle. For example, Yamaha RMAX is controlled by communicating with the built-in flight control system called YACS (Yamaha Attitude Control System) over serial port while Maxi-Joker is controlled by directly sending the PWM signals to the servos using an MFIB. Figure 8 shows the difference between these platforms. These vehicles have different dynamic response and the control gains and therefore other associated limiting values have to be adjusted accordingly. The existing code set that has been used since the beginning of our Berkeley UAV project in 1997 had accumulated, as any other software development would, quite large amount of defunct or obsolete code pieces. Some other part of the program was hardcoded to the target hardware at the time of the development, which makes the upgrade or customization to different configuration makes very painful and error-prone. To facilitate smooth and accurate customization to the target system while preserving the capabilities such as waypoint navigation and more, the flight control software mentioned in the previous section has been re-architected and rewritten in C++ for improved modularity and ease of further development. Also, the vehicle-specific values are all defined in a separate header file so that the required changes will be made in the designated

header files and not anywhere else. Leveraging on this recent improvements, the migration to RMAX platform is anticipated least painful and time-consuming, since the involved changes will be made on the interfacing and adjusting vehicle-specific parameters. The servo interface part for Maxi-Joker is based on serial communication to the MFIB, which will be replaced with a code set also based on serial communication but in different message format defined by Yamaha. The receiver interfacing part is also adjusted in a similar manner. The control gains and a few vehicle specific parameters will be programmed in the vehicle-specific header file.

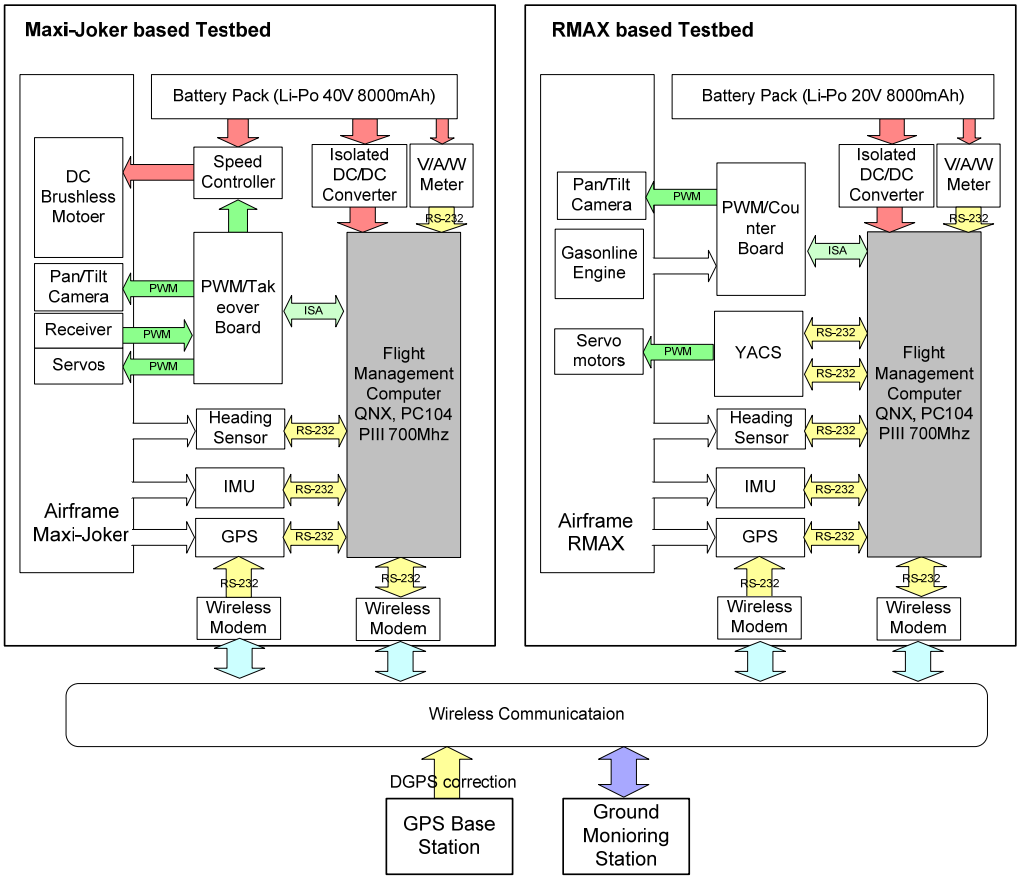

Figure 8. Schematic diagram of hardware architecture of Joker-based avionics (left) and RMAX-based avionics (right)

VI. Conclusion

In this work, we developed a target designation control system using a small helicopter UAV. We first derived equations to define the relationship between the helicopter's motion and the end-point's deviation. Using the derived equations, a control strategy to improve the targeting accuracy is proposed. A lightweight helicopter UAV is developed and put into a conventional hover test to collect flight data to assess the current target tracking capability and to estimate the error budget. A series of flight test will be performed using the proposed controller design soon. A roadmap for the migration to Yamaha RMAX is also given; the required work will be reduced to minimal due to the recent code restructuring as described above.

VII. Papers submitted

D. H. Shim and S. Sastry, "A High- precision Targeting System Design using a Helicopter UAV," AIAA Guidance, Navigation, and Control Conference, 2007 (To appear)

References

[1]Joint PUB 3-09.1, *Joint Laser Designation Procedures* (JLASER), June 1991.

[2]D. H. Shim, *Hierarchical Control System Synthesis for Rotorcraft-based Unmanned Aerial Vehicles,* Ph. D. thesis, University of California, Berkeley, 2000.

[3]D. H. Shim, H. J. Kim, S. Sastry, "Hierarchical Control System Synthesis for Rotorcraft-based Unmanned Aerial Vehicles", *AIAA Guidance, Navigation and Control Conference*, Denver, August 2000.

[4]D. H. Shim and S. Sastry, "A Situation-aware Flight Control System Design using Real-time Model Predictive Control for Unmanned Autonomous Helicopters," AIAA Guidance, Navigation, and Control Conference, Keystone, CO, 2006.

[5]R. Vidal, O. Shakernia, H. J. Kim, H. Shim, S. Sastry, "Multi-Agent Probabilistic Pursuit-Evasion Games with Unmanned Ground and Aerial Vehicles," *IEEE Transactions on Robotics and Automation*, vol.18, no. 5, pages 662-669, October 2002.

[6]T. Templeton, D. H. Shim, and S. Sastry, "Autonomous Vision-based Terrain Mapping using an Unmanned Aerial Vehicle," to appear in International Conference on Robotics and Automation, 2007.